

# Thermal decomposition studies of $[\text{Ni}(\text{NH}_3)_6]\text{X}_2$ ( $\text{X} = \text{Cl}, \text{Br}$ ) in the solid state using TG-MS and TR-XRD

K. S. Rejitha · T. Ichikawa · S. Mathew

Received: 22 April 2010/Accepted: 14 September 2010/Published online: 8 October 2010  
© Akadémiai Kiadó, Budapest, Hungary 2010

**Abstract** Detailed investigation on the thermal behaviour of hexaamminenickel(II) chloride and hexaamminenickel(II) bromide has been carried out by means of simultaneous TG/DTA coupled online with mass spectroscopy (TG-MS) and temperature-resolved X-ray diffraction (TR-XRD). Evolved gas analyses by TG-MS revealed the presence of  $\text{NH}_2$ ,  $\text{NH}$ ,  $\text{N}_2$  and  $\text{H}_2$  fragments in addition to ammonia during the deamination process. These transient species resulted due to the fragmentation of the evolved ammonia during pyrolysis. The intermediates formed during the thermal deamination stages were monitored by in situ TR-XRD. The final product of the decomposition was found to be nano size metallic nickel in both cases. Morphology of the complexes, intermediates and the residue formed at various decomposition stages was analysed by scanning electron microscope (SEM). Kinetic analyses using isoconversional method for deamination and dehalogenation reaction show that the activation energies vary with the extent of conversion, indicating the multi-step nature of these solid state decomposition reactions.

**Keywords** TG-MS · TR-XRD · SEM · Nano nickel · Kinetics · Isoconversional methods

## Introduction

Thermal decomposition studies of transition metal amine complexes have extensively been investigated over years [1–3]. A scan through the literature reveals that various reports are available regarding the description of the evolved gaseous species and the transient intermediates formed during thermal deamination [3, 4]. Albeit these conflicting reports, mostly all the studies take a simplified approach in dealing the interpretations of the thermal fragments during the deamination process, as all these studies were enabled only with the aid of TG/DTA for thermal analysis. Therefore, it was felt imperative to have a detailed investigation on the evolved gaseous products to ascertain the nature of the fragmented species without any ambiguity and the structural/phase changes if any occurring during the deamination event. A detailed investigation of this sort warrants the use of techniques like thermogravimetric-mass spectroscopy (TG-MS) and temperature-resolved X-ray diffraction (TR-XRD).

Conventional thermoanalytical techniques like TG, DTA and DSC do not tell the nature of the gaseous products. Evolved gas analysis (EGA) offers a useful tool to identify the fragments which cannot be detected by other techniques [5, 6]. TR-XRD is a powerful tool to study the structural/phase changes occurring during a solid state reaction as well as in identifying the reaction intermediates in situ during pyrolysis. This method enables the recording of a series of pattern, while the samples are heated continuously, stepwise or isothermally during the reaction. These series contain information on the lattice of solids and on the structural changes as a function of temperature [7].

The present investigation aims to explore a detailed thermal decomposition behaviour of hexaamminenickel(II) chloride and hexaamminenickel(II) bromide in the aforementioned

K. S. Rejitha · S. Mathew (✉)  
School of Chemical Sciences, Mahatma Gandhi University, P.D.  
Hills P.O., Kottayam, Kerala 686 560, India  
e-mail: sureshmathews@sancharnet.in

T. Ichikawa  
Institute for Advanced Materials Research, Hiroshima  
University, Higashi-Hiroshima 739-8530, Japan

context. To the best of our knowledge, TG-MS studies on the nature of the gaseous species evolved and the TR-XRD studies on the structural changes happening during the thermal decomposition of the title complexes have not been reported. Thermolysis of materials often leads to the formation of metal oxides or metals in the nano range [8, 9]. Mathew et al. [2] have reported the formation of ultrafine metallic copper wires by the thermal decomposition of tris(ethylenediamine)copper(II) halides. Syntheses of nano NiO or Ni by the thermal decomposition of nickel complexes have also been reported [10, 11]. These findings are of importance as it opens up a strategy for the synthesis of ultrafine nano metals and metallic oxides with controlled morphology in contemporary material research. This aspect also makes the thermal decomposition studies of amine complexes quite significant. The kinetics of deamination and dehalogenation of hexaamminenickel(II) halides have been studied using model-free isoconversional methods viz., Flynn–Wall–Ozawa (FWO) [12, 13], Friedman [14] and Kissinger–Akahira–Sunose (KAS) [15, 16].

## Experimental

The nickel ammine halide complexes were synthesized as per the procedure reported in the literature [17]. Nickel content in the complexes was determined by gravimetry [18]. The complexes were further characterized by spectral and chemical analysis. The halide content in the complexes was determined by Volhard's method [18].

### Instrumentations

TG-MS studies were carried out in a thermogravimetric apparatus (TG; Rigaku, TG-8120) combined with mass spectroscopy (Anelva, M-QA200TS) under high-purity He gas flow (99.9999%). The heating rates employed were 5, 10, 15 and 20 K min<sup>-1</sup>. For the TG/DTA analyses, the sample mass used were 10 ± 0.2 mg for all the experiments.

The elemental analyses were carried out using Vario Elemental III instrument. X-ray powder patterns were recorded on a Bruker D8 Advance diffractometer attached with a programmable temperature device from Anton Paar (TTK 450) up to 400 °C (using Cu K<sub>α</sub> radiation,  $\lambda = 1.542 \text{ \AA}$ ). The measurements were performed by placing the sample on a flat sample holder, while the samples were heated by a programmable temperature controller. Crystallite size was calculated using the Scherrer equation,

$$t = 0.9\lambda/\beta \cos \theta,$$

where  $t$  is the thickness of the particle,  $\lambda$  is the wave length,  $\beta$  is the line broadening (in radians) and  $\cos \theta$  is the corresponding angle. Morphology of the complexes, intermediates and

residues were determined using JEOL JSM-6390 scanning electron microscope (SEM). For SEM analyses, the samples were spread on a carbon tape and made uniform by blowing air.

### Kinetic studies

#### *Isoconversional methods*

Solid state reaction often follows the basic kinetic equation

$$\frac{d(\alpha)}{dt} = A \exp \frac{-E}{RT} f(\alpha), \quad (1)$$

where  $A$  is the pre-exponential factor,  $E$  is the activation energy,  $R$  is the gas constant and  $T$  is the temperature,  $f(\alpha)$  is the kinetic model function. For a non-isothermal reaction, Eq. 1 can be written as

$$\frac{d(\alpha)}{f(\alpha)} = \frac{A}{\phi} \exp \frac{-E}{RT} dT, \text{ where the heating rate } \phi = \frac{dT}{dt}. \quad (2)$$

The solid state reactions involve complex reaction steps, and a single rate equation is unable to explain the complexities of solid state reactions. In this context, isoconversional method could be used as an alternative to study the solid state reactions. Model-free isoconversional methods are a versatile way to investigate the kinetics of solid state reactions as these methods possess several advantages over the conventional methods [19–22]. For a single step reaction,  $E$  is constant over the whole conversion function. For multi-step kinetics,  $E$  varies with the extent of conversion, and this reflects the variation in relative contributions of single steps to the overall reaction rate. Friedman, FWO and KAS are isoconversional methods and are frequently employed to study the kinetics. These methods yield effective activation energy ( $E$ ) as a function of extent of conversion ( $\alpha$ ).

In order to study the kinetics using the model-free methods, several TG measurements were carried out at different heating rates. Friedman, Flynn–Wall–Ozawa (FWO) as well as Kissinger–Akahira–Sunose (KAS) methods are based on multiple heating rate experiments.

Flynn–Wall–Ozawa equation is as follows [12, 13]

$$\ln \phi = \ln \frac{AE}{R} - \ln g(\alpha) - 5.3305 - 1.052 \frac{E}{RT} \quad (3)$$

where  $\phi$  is the heating rate,  $\alpha$  is the degree of conversion,  $g(\alpha)$  is the mechanism function,  $E$  is the activation energy,  $A$  is the pre-exponential factor and  $R$  is the gas constant.

Friedman equation is [14]

$$\ln \frac{d\alpha}{dt} = \ln[Af(\alpha)] - \frac{E}{RT}, \quad (4)$$

where  $d\alpha/dt$  is the rate of conversion and  $f(\alpha)$  is the mechanism function.

Kissinger–Akahira–Sunose (KAS) equation is [15, 16]

$$\ln\left(\frac{\phi}{T^2}\right) = \ln\frac{AR}{Eg(\alpha)} - \frac{E}{RT}. \quad (5)$$

From the above Eqs 3–5 the plots of  $\ln \phi$  versus  $1/T$ ,  $\ln d\alpha/dt$  versus  $1/T$ ,  $\ln \phi/T^2$  versus  $1/T$  give straight lines with slopes  $-1.052E/R$ ,  $-E/R$  and  $-E/R$ , respectively, for the FWO, Friedman and KAS equations. The slope of the straight lines is directly proportional to the activation energy.

## Results and discussion

### TG-MS studies of hexaamminenickel(II) halide complexes

The results of elemental analyses are shown in Table 1 and are in good agreement with those calculated theoretically, which confirm the formation of the complexes. The phenomenological details like temperature of inception  $T_i$ , final temperature  $T_f$  and the temperature of summit  $T_s$  for the thermal decomposition of hexaamminenickel(II) halide complexes and the mass loss data are given in Table 2. The plot of simultaneous TG/DTA coupled online with MS for  $[\text{Ni}(\text{NH}_3)_6]\text{Cl}_2$  is given in Fig. 1. From the TG plot, it is seen that the first stage of thermal decomposition of hexaamminenickel(II) chloride is in the temperature range 79–140 °C and this stage corresponds to the release of four ammonia molecules. Mass spectra show a strong peak with  $m/z$  value 17, signaturing the presence of ammonia molecules at 132 °C because of this deamination reaction. Also

the DTA shows an endotherm with  $T_p$  136 °C corresponding to this deamination stage. Broadly, the second stage of decomposition comprises the release of two ammonia molecules in the temperature range 140–280 °C. (However, a very slow mass loss is observed in the TG depicting the partial release of ammonia in the temperature regime 140–200 °C. A close perusal of the DTA curve shows a small endothermic ( $T_p = 185$  °C) peak indicating this slight mass loss of 2%.) The MS peak ( $m/z$  17) with very low intensity at 184 °C and an intense ion peak ( $m/z$  17) at 266 °C substantiate the above observation. This second stage of deamination ( $-2\text{NH}_3$ ) resulted in the formation of  $\text{NiCl}_2$  (mass loss 14.3%) as shown in Table 2.

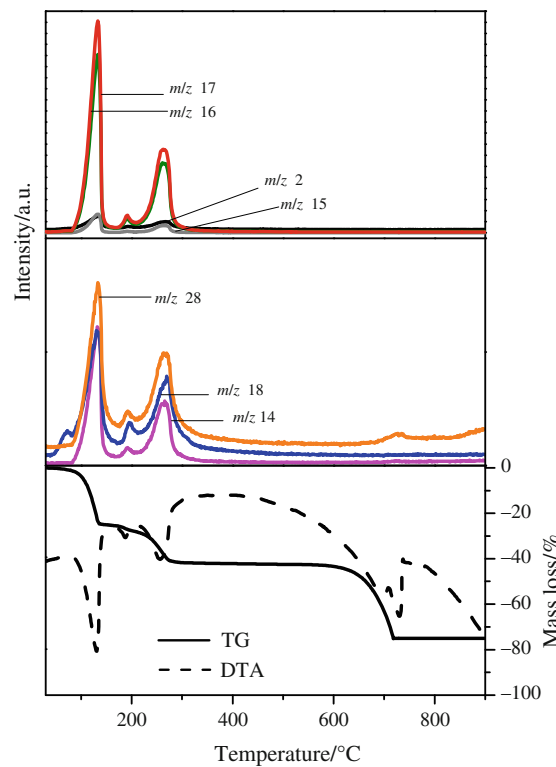


**Fig. 1** TG/DTA-MS plot for hexaamminenickel(II) chloride at heating rate  $10\text{ }^\circ\text{C min}^{-1}$

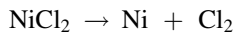
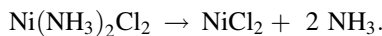
**Table 1** Elemental analysis/%

Complexes	Ni obsd/ calcd	H obsd/ calcd	N obsd/ calcd	Halogen obsd/calcd
$[\text{Ni}(\text{NH}_3)_6]\text{Cl}_2$	24.9/25.3	8.1/7.8	36.1/36.3	31.1/30.6
$[\text{Ni}(\text{NH}_3)_6]\text{Br}_2$	17.8/18.3	6/5.7	26.6/26.2	50.1/49.9

**Table 2** Phenomenological data for the thermal decomposition of hexaamminenickel(II) halides/ $\phi = 10\text{ }^\circ\text{C min}^{-1}$

Complexes	Stages	TG results			Percentage mass loss				Residue
		$T_i/^\circ\text{C}$	$T_f/^\circ\text{C}$	$T_s/^\circ\text{C}$	Theoretical Stepwise	Observed	Theoretical Cumulative	Observed	
$[\text{Ni}(\text{NH}_3)_6]\text{Cl}_2$	1	79	140	132	29.3	28.9	29.3	28.9	$\text{Ni}(\text{NH}_3)_2\text{Cl}_2$
	2	140	280	250.7	14.7	14.3	44	43.2	$\text{NiCl}_2$
	3	609	743.8	727.8	30.6	31.8	74.6	75	Ni
$[\text{Ni}(\text{NH}_3)_6]\text{Br}_2$	1	90	180	155.5	21.2	21	21.2	21	$\text{Ni}(\text{NH}_3)_2\text{Br}_2$
	2	180	260	239.6	10.6	10	31.8	31	$\text{NiBr}_2$
	3	580.5	726.7	716.8	49.9	49	81.7	80	Ni

The decomposition of  $\text{NiCl}_2$  commences at 609 °C and the mass loss of 31.8%, corresponding to the release of chlorine resulted in the formation of metallic nickel at 744 °C as the residue. However, the evolution of  $\text{Cl}_2$  or its fragments during the final stage of thermal decomposition is not detected in the TG-MS. The DTA curve shows an endotherm at 740 °C corresponding to the dechlorination reaction. The overall thermal decomposition pattern for hexaamminenickel(II) chloride can be written as follows:



However, Tanaka et al. have reported that the two ammonia molecules are released in two successive steps, and  $\text{NiCl}_2\text{-NH}_3$  is formed as an intermediate. According to this report, the formation of  $\text{NiCl}_2\text{-NH}_3$  takes place only at relatively lower heating rates [23]. Since the TG-MS analysis in the present study was done at 10 °C min<sup>-1</sup>, no distinct and well-separated stages of deamination ( $-\text{NH}_3$ ) is observed.

TG-MS analysis shows ion peaks with mass numbers 2, 14, 15, 16 and 28. These mass numbers indicate the presence of fragments like H<sub>2</sub>, N, NH, NH<sub>2</sub> and N<sub>2</sub>, respectively. These species can be formed due to the fragmentation of the liberated ammonia during pyrolysis [24, 25].

The plot of simultaneous TG/DTA coupled online with MS for  $[\text{Ni}(\text{NH}_3)_6]\text{Br}_2$  is shown in Fig. 2. The thermal

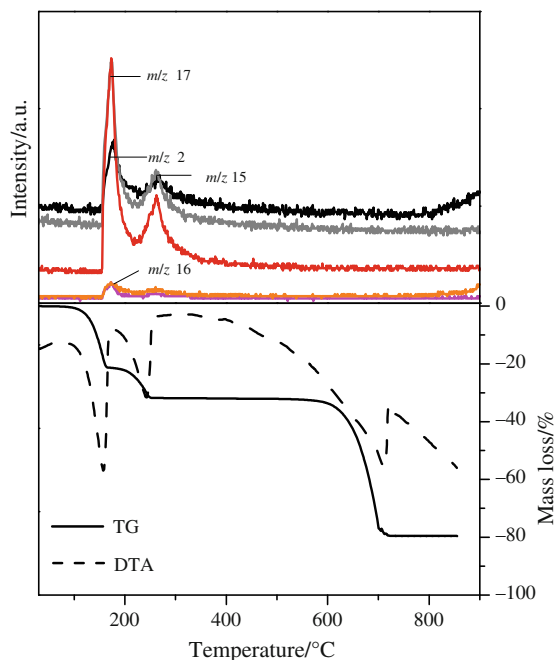
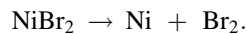
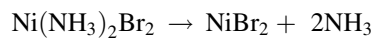
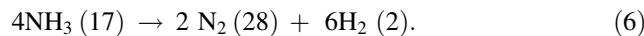


**Fig. 2** TG/DTA-MS plot for hexaamminenickel(II) bromide at heating rate 10 °C min<sup>-1</sup>

decomposition of hexaamminenickel(II) bromide starts at 90 °C with the loss of four molecules of ammonia and this is evidenced by the MS ion peak at 165 °C. The second stage of deamination involves the liberation of two ammonia molecules in the temperature range 180–260 °C, and the corresponding ion peak with mass number 17 (in Fig. 2) at 250 °C indicates the evolution of two ammonia molecules. The observed intensity of the two MS peaks is consistent with the amount of ammonia released viz., four molecules of ammonia in the first stage and two molecules of ammonia in the second stage of thermal decomposition. The final mass loss of 49% corresponds to the formation of metallic nickel as the final product of thermal decomposition. The liberation of Br<sub>2</sub> or its fragments, during the final stage of decomposition, is not detected by the mass spectral analysis. Corresponding thermal decomposition stages appear as three endothermic peaks in DTA. From the TG-MS data, the decomposition of hexaamminenickel(II) bromide is shown below.



MS analysis has also detected peaks with *m/z* values 2, 18 and 28. The ion peak 18 may be due to the adsorbed moisture. The other two peaks with mass numbers 2 and 28 may be due to H<sub>2</sub> and N<sub>2</sub> fragments formed by the decomposition of ammonia as shown below.



Peaks with mass number 15 and 16 in the mass spectra indicate the formation of NH and NH<sub>2</sub> species formed by the fragmentation of ammonia.

#### TR-XRD studies of hexaamminenickel(II) halide complexes

For complementing the TG-MS analysis, in situ TR-XRD studies were done for the first time to probe the structure/stability of the phases formed during the deamination stages. The non-isothermal X-ray diffraction series (40–400 °C) is shown in Fig. 3. The TR-XRD pattern in the range 40–60 °C contains characteristic peaks corresponding to (111), (220), (222), (400) and (422) planes of this complex (JCPDS no. 24-0803). On heating peaks corresponding to these planes disappear to form new lattice planes corresponding to the formation of diammine complex by the loss of four molecules of ammonia. The pattern at 120 °C is the intermediate structure between parent hexaammine complex and the diammine species. The pattern obtained at 140 °C represents the diammine species. Peaks with two  $\theta$  values 15.7, 20, 30.2, 35.5 and 40.6

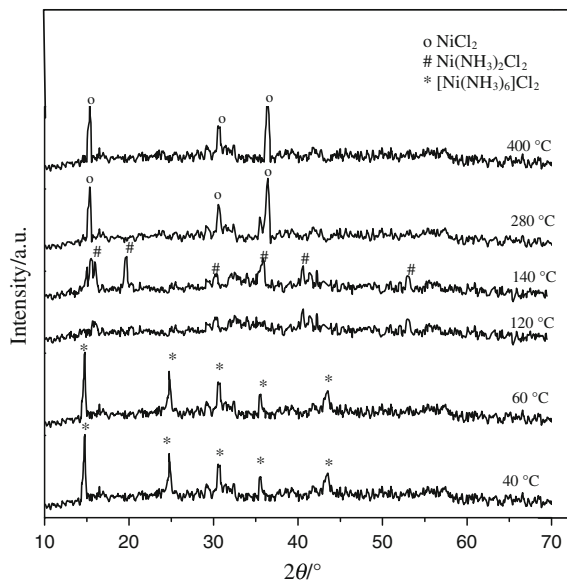


**Fig. 3** TR-XRD pattern for  $[\text{Ni}(\text{NH}_3)_6]\text{Cl}_2$

of the diammine complex are in agreement with reported refinement data of diamminenickel(II) chloride [26]. The diammine complex is not stable and suddenly undergoes decomposition by the release of two ammonia molecules. At 280 °C, peaks corresponding to (003), (101) and (104) planes of  $\text{NiCl}_2$  (JCPDS no. 71-2032) lattice start to appear by the loss of remaining ammonia molecules. TG-MS data also show ion peak corresponding to the evolution of ammonia at this stage.  $\text{NiCl}_2$  begins to decompose above 400 °C to give Ni as the final residue. This is not recorded as the temperature limit of the heating attachment of the sample holder for TR-XRD is up to 400 °C. In order to identify the final residue, the complex was heated in a muffle furnace maintaining similar conditions as in a TG furnace. Figure 4 shows the XRD pattern of the residue,

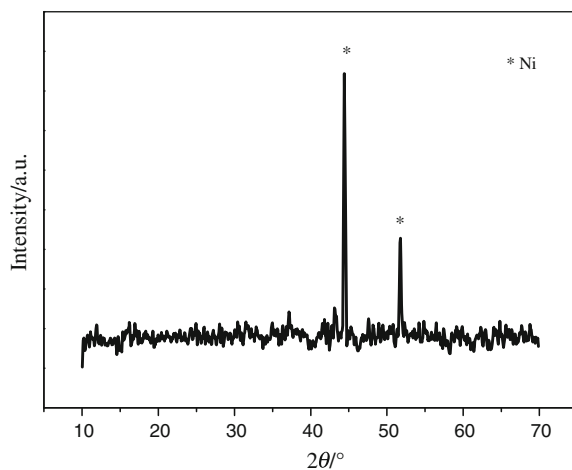


**Fig. 4** XRD pattern for metallic nickel formed from  $[\text{Ni}(\text{NH}_3)_6]\text{Cl}_2$

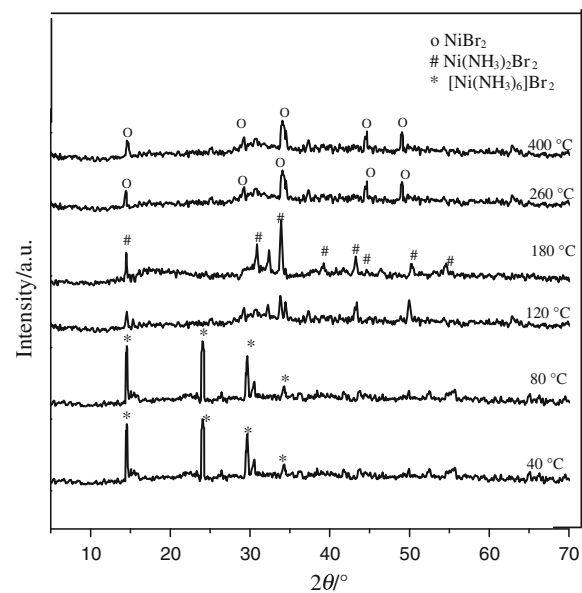


**Fig. 5** TR-XRD pattern for  $[\text{Ni}(\text{NH}_3)_6]\text{Br}_2$

which shows the characteristic planes of metallic nickel (JCPDS no. 04-0850). The average crystallite size of the residue calculated by the Scherrer equation is found to be  $\sim 20$  nm.

The TR-XRD pattern of  $[\text{Ni}(\text{NH}_3)_6]\text{Br}_2$  is shown in Fig. 5. The patterns at 40–80 °C contain the peaks corresponding to (111), (220), (222) and (400) planes of  $[\text{Ni}(\text{NH}_3)_6]\text{Br}_2$  (JCPDS no. 24-0802). As the temperature increases, all the planes except (111) plane of the hexaammine complex disappear and new peaks start to appear, this is due to the loss of ammonia from the hexaammine complex. The TR-XRD pattern at 120 °C contains the (111) plane of the hexaammine complex with lower intensity. The pattern at 180 °C is due to the formation of  $\text{Ni}(\text{NH}_3)_2\text{Br}_2$  by the loss of four molecules of ammonia as evident from TG analysis. The diammine species also contain the (111) plane of the hexaammine complex with lower intensity. TR-XRD results show that (111) planes of the parent hexaammine complex become part of the intermediate as well as the diammine complex lattice as can be seen from the lowering of intensity of this peak in the temperature range 100–180 °C. The main peaks obtained for diamminenickel(II) bromide at  $2\theta$  values 30.9, 32.6, 34.0, 39.2 and 44.5 match well with the reported values [26]. The evolution of ammonia is confirmed by the TG-MS results. Diammine complex is very unstable and starts to decompose above 180 °C and ends at 260 °C by the release of two ammonia molecules. TG-MS detected the liberation of ammonia at this temperature range. At 260 °C, peaks corresponding to  $\text{NiBr}_2$  appear. The formation of planes corresponding to (003), (101), (104), (107) and (110) at 260 °C confirm the presence of  $\text{NiBr}_2$ .

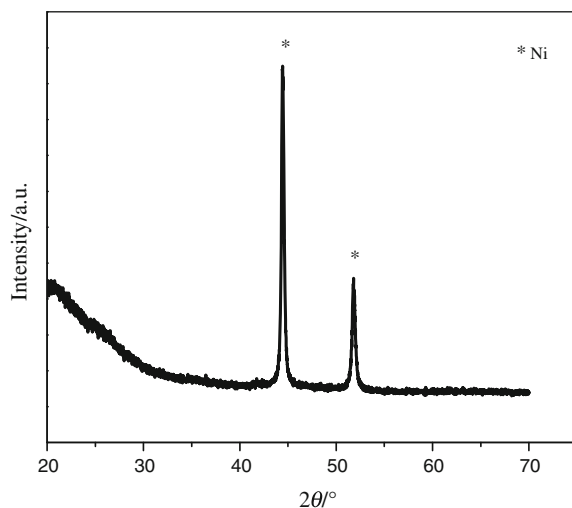


**Fig. 6** XRD pattern for metallic nickel formed from  $[\text{Ni}(\text{NH}_3)_6]\text{Br}_2$

(JCPDS no. 73-0331). The final residue was separated by heating the complex in a muffle furnace and analysed by XRD. The pattern in Fig. 6 shows the presence of well-crystalline fcc structure of nickel. The average crystallite size of the residue calculated from the peak broadening value is found to be 20 nm.

#### SEM analyses of the complexes

The SEM pictures of the complexes, intermediates and the residue formed during thermal decomposition of  $[\text{Ni}(\text{NH}_3)_6]\text{Cl}_2$  and  $[\text{Ni}(\text{NH}_3)_6]\text{Br}_2$  are shown in Figs. 7 and 8, respectively. All the decomposition products in each stage were separated by heating the complex under identical heating rate in a programmable muffle furnace simulating the conditions of thermogravimetric experiments. SEM pictures show that both the complexes appear as octahedral crystals and the surfaces of the octahedra correspond to (111) plane [27], while there is considerable morphological change occurring for these complexes during heating. Even though, the intermediates  $\text{Ni}(\text{NH}_3)_2\text{Cl}_2$  (Fig. 7b) and  $\text{NiCl}_2$  (Fig. 7c) formed from  $[\text{Ni}(\text{NH}_3)_6]\text{Cl}_2$  retain the octahedral structure, the topology of the surfaces seems to be not as smooth as the original complex. Literature reports reveal that the intermediates of hexaamminenickel(II) chloride possess polymeric pseudo octahedral geometry [23]. In  $\text{Ni}(\text{NH}_3)_2\text{X}_2$  ( $\text{X}$  = halogens), each nickel ion is considered to be surrounded by four bridging halogens in a square planar configuration and two ammonia molecules located in trans position. Nickel ion keeps the coordination number of six throughout the decomposition process when ammonia molecules are replaced stepwise by halogens [23]. The porous structure can be due to the release of ammonia from the complex.

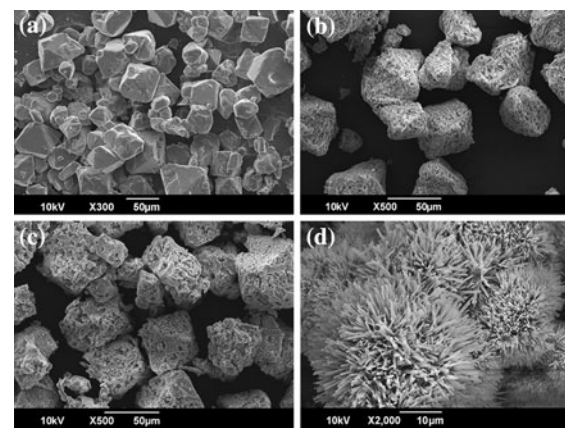


**Fig. 7** SEM images of **a**  $[\text{Ni}(\text{NH}_3)_6]\text{Cl}_2$ , **b**  $\text{Ni}(\text{NH}_3)_2\text{Cl}_2$ , **c**  $\text{NiCl}_2$ , **d** Ni

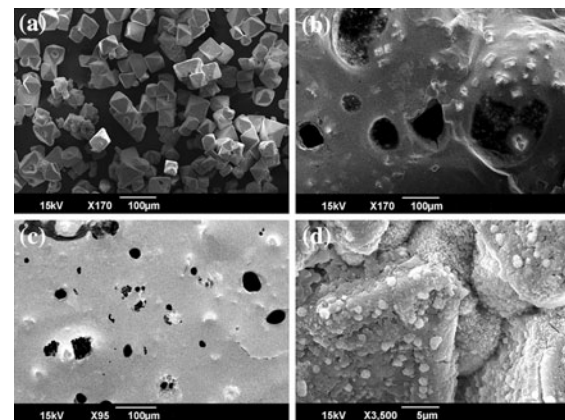


**Fig. 8** SEM images of **a**  $[\text{Ni}(\text{NH}_3)_6]\text{Br}_2$ , **b**  $\text{Ni}(\text{NH}_3)_2\text{Br}_2$ , **c**  $\text{NiBr}_2$ , **d** Ni

The final residue, i.e. nickel metal, appears as flower-shaped nano structure (Fig. 7d). SEM images show the porous nature of  $\text{Ni}(\text{NH}_3)_2\text{Br}_2$  (Fig. 8b).  $\text{NiBr}_2$  is also showing a porous structure (Fig. 8c), but it looks denser than its precursor. These pores may be formed due to the release of ammonia from the surfaces during heating. Similar porous structures have been reported during the thermal decomposition of  $[\text{Ni}(2\text{-picolylamine})_2(\text{NO}_3)_2]$  due to the elimination of NO [28]. The final residue appears as agglomerated and is shown in Fig. 8d. Morphology difference arises since these residues are formed from two different precursors namely  $\text{NiCl}_2$  and  $\text{NiBr}_2$ .

It is found that the size and morphology of nickel nanoparticles can be tailored by merely changing the precursors. In this way, thermal decomposition can be used as a facile and effective route for the synthesis of nano materials with controlled morphology and this is quite significance as the morphology and the size influence their

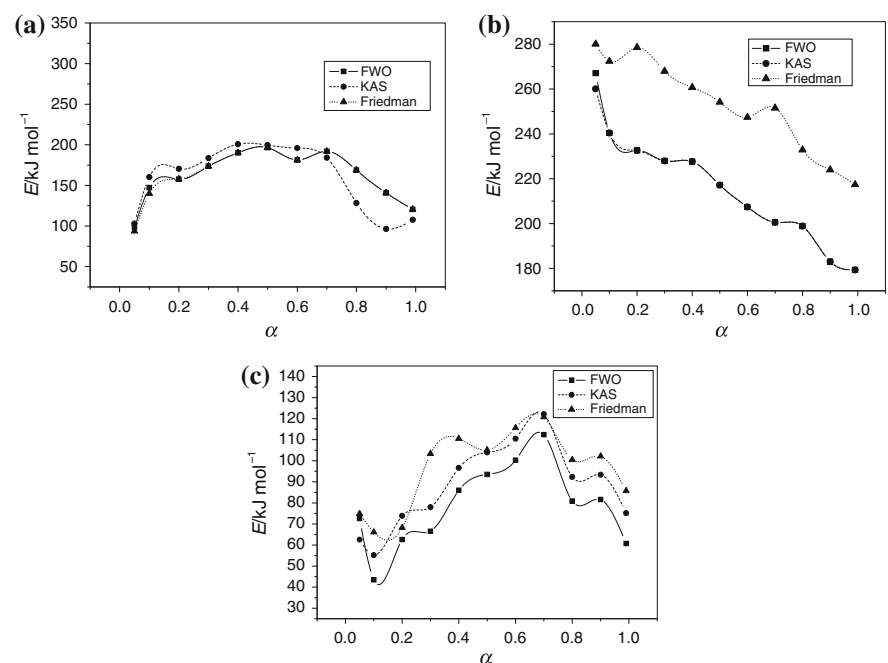
physical properties. Nickel nanoparticles have interesting magnetic properties and have the potential in the usage as data storage devices and in ferrofluids [29].

#### Kinetic studies of hexaamminenickel(II) halide complexes

The activation energies of the decomposition were calculated using isoconversional methods. Isoconversional methods help to calculate activation energy as a function of conversion without the prediction of a reaction model. Existence of the dependence of  $E$  on conversion ( $\alpha$ ) is an indication on the multi-step solid state reaction. The effective activation energy of the process is a composite value determined by the activation energies of elementary steps as well as by the relative contributions of these steps to the over all reaction rate. The contributions of the individual steps can change with the extent of conversion as well as with the temperature. Hence, the variation of  $E$  with  $\alpha$  is an indication of multi-step kinetics [30]. From the dependence of activation energy on the extent of conversion, the nature of solid state reactions can be predicted.

The results of kinetic analyses calculated using isoconversional methods for the complexes are given in Figs. 9a–c and 10a–c. In the case of hexaamminenickel(II) chloride, for the first deamination step (Fig. 9a) the activation energy (calculated by FWO and KAS methods) increases in the  $\alpha$  range 0.1–0.45 and then decreases after 0.45. The increasing dependence of  $E$  on  $\alpha$  shows that the reaction is competing or consecutive. Solid state reaction of the type solid  $\rightarrow$  solid + gas undergo such type of reactions [31].

**Fig. 9** Variation of  $E$  with  $\alpha$  for **a** deamination, **b** deamination and **c** dechlorination for  $[\text{Ni}(\text{NH}_3)_6]\text{Cl}_2$

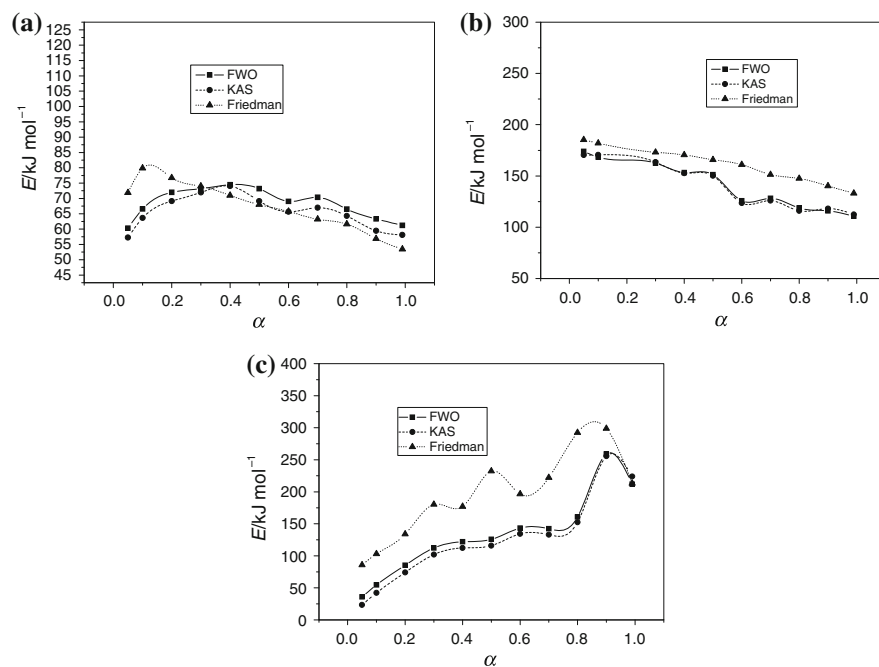


The decrease in  $E$  from 0.45 till the end of the reaction may be an indication of the mass transfer-controlled diffusion mechanism [30]. The second deamination stage also shows a decreasing tendency of  $E$  with  $\alpha$ . It is reported that the kinetics of the decomposition of hexaammine complex is limited by the heat and mass transfer through the porous surfaces which is formed during the decomposition process [32]. For the dechlorination step (Fig. 9c), the activation energy increases in the  $\alpha$  range 0.1–0.65 and decreases after 0.65. Millan et al. [32] have reported that the decomposition of the hexaammine complex is due to the pressure of the desorbed ammonia gas which leads to the collapse of the structure at point, line or plane defects.

For hexaamminenickel(II) bromide, first deamination (Fig. 10c) shows increasing dependence of  $E$  in the  $\alpha$  range 0.05–0.4, thereafter the value of  $E$  is found to be decreasing. The second deamination step shows a decreasing value of  $E$  with  $\alpha$ . The decrease in the activation energy indicates the mass transfer controlled diffusion mechanism. For the debromination step (Fig. 10c), activation energy increases in the  $\alpha$  range 0.05–0.85 and then tends to decrease. As mentioned above, the increasing dependence of  $E$  on  $\alpha$  shows that the reaction is competing or consecutive.

It is seen that the activation energy calculated by FWO and KAS methods are comparable. However, the activation energies calculated by Friedman method show higher values in most cases. This is because the Friedman method is very sensitive to experimental noise and tends to be numerically unsound when employing instantaneous rate values [33].

**Fig. 10** Variation of  $E$  with  $\alpha$  for **a** deamination, **b** deamination and **c** debromination of  $[\text{Ni}(\text{NH}_3)_6]\text{Br}_2$



## Conclusions

Evolved gas analysis by mass spectra of the nickel ammine bromide and chloride complexes reveal that along with ammonia other species like  $\text{N}_2$ ,  $\text{H}_2$ ,  $\text{NH}_2$  and  $\text{NH}$  are also evolved during the pyrolysis which are formed from the fragmentation of the evolved ammonia. The different intermediates and the residues formed were analysed by TR-XRD and the results complement with the TG-MS observation. The morphology of the complexes, intermediates and the residues were analyzed by SEM. The SEM images show the porous nature of the intermediates formed during thermal decomposition of these complexes due to the liberation of ammonia. Both the nickel ammine bromide and chloride complexes produce metallic nickel in the nano size range as the final product with different morphology. Thermal decomposition kinetics of the complexes were studied by isoconversional methods. It was revealed that the activation energy varies with the extent of conversion, indicating the multi-step nature of thermal decomposition of these ammine complexes.

**Acknowledgements** The authors are grateful to the Sophisticated Test and Instrumentation Centre (STIC), Cochin, for recording TR-XRD patterns.

## References

- Wendlandt WW, Smith JP. Thermal properties of transition metal amine complexes. Amsterdam: Elsevier; 1967.
- Mathew S, Nair CGR, Ninan KN. Thermal decomposition kinetics: kinetics and mechanism of thermal decomposition of bis(ethylenediamine)copper(II) halide monohydrate. *Thermochim Acta*. 1991;181:253–68.
- Singh G, Pandey DK. Studies on energetic compounds: kinetics of thermal decomposition of nitrate complexes of some transition metals with propylenediamine. *Combust Flame*. 2003;135:135–43.
- Mathew S, Nair CGR, Ninan KN. Thermal decomposition kinetics: kinetics and mechanism of thermal decomposition of tetraamminecopper(II) sulphate monohydrate. *Thermochim Acta*. 1989;144:33–43.
- Madara'sz J. Evolved gas analyses on a mixed valence copper (I, II) complex salt with thiosulfate and ammonia by in situ TG-EGA-FTIR and TG/DTA-EGA-MS. *J Therm Anal Calorim*. 2009;97:111–6.
- Sanders JP, Gallagher PK. Kinetic analysis of complex decomposition reactions using evolved gas analysis. *J Therm Anal Calorim*. 2009;96:805–11.
- Mathew S, Eisenreich N, Engel W. Thermal analysis using X-ray diffractometry for the investigations of the solid state reaction of ammonium nitrate and copper oxide. *Thermochim Acta*. 1995;269/270:475–89.
- Nair PS, Scholes GD. Thermal decomposition of single source precursors and the shape evolution of CdS and CdSe nanocrystals. *J Mater Chem*. 2006;16:467–73.
- Navaladian S, Viswanathan B, Viswanath RP, Varadarajan TK. Thermal decomposition as a route for silver nanoparticles. *Nanoscale Res Lett*. 2007;2:44–8.
- Li X, Zhang X, Li Z, Qian Y. Synthesis and characteristics of NiO nanoparticles by thermal decomposition of nickel dimethylglyoximate rods. *Solid State Commun*. 2006;137:581–4.
- Chen Y, Peng D, Lin D, Luo X. Preparation and magnetic properties of nickel nano particles via thermal decomposition of nickel organometallic precursors in alkylamine. *Nanotechnology*. 2007;18:505703–8.
- Ozawa T. A new method of analyzing thermogravimetric data. *Bull Chem Soc Jpn*. 1965;38:1881–6.
- Flynn JH, Wall LA. A quick, direct method for the determination of activation energy from thermogravimetric data. *J Polym Sci B*. 1996;4:323–8.
- Friedman HL. New methods for evaluating kinetic parameters from thermal analysis data. *J Polym Sci B*. 1969;7:41–6.

15. Kissinger HE. Reaction kinetics in differential thermal analysis. *Anal Chem.* 1957;29:1702–6.
16. Akahira T, Sunose T. Research report of Chiba Institute Technology. 1971;16:22–31.
17. Brauer G. Hand book of preparative inorganic chemistry. 2nd ed. New York: Academic Press; 1965.
18. Vogel AG. Text book of quantitative inorganic analysis. 4th ed. London, UK: Longmann; 1978.
19. Badrinarayanan P, Zheng W, Simon SL. Isoconversional analysis of the glass transition. *Thermochim Acta.* 2008;468:87–93.
20. Curtis SD, Kubiak M, Kurdziel K, Materazzi S, Vecchio S. Crystal structure and thermoanalytical study of a cadmium(II) complex with 1-allylimidazole. *J Anal Appl Pyrolysis.* 2010;87: 175–9.
21. Cai JM, Bi LS. Kinetic analysis of wheat straw pyrolysis using isoconversional methods. *J Therm Anal Calorim.* 2009;98: 325–30.
22. Su TT, Zhai YC, Jiang H, Gong H. Studies on the thermal decomposition kinetics and mechanism of ammonium niobium oxalate. *J Therm Anal Calorim.* 2009;98:449–55.
23. Tanaka N, Kagawa M, Kamada M. The thermal decomposition of hexaamminenickel(II) complexes. *Bull Chem Soc Jpn.* 1968;41: 2908–13.
24. Madarasz J, Bombicz P, Matyas C, Reti F, Kiss G, Pokol G. Comparative evolved gas analytical and structural study on *trans*-diammine-bis(nitrito)-palladium(II) and platinum(II) by TG/DTA-MS, TG-FTIR and single crystal X-ray diffraction. *Thermochim Acta.* 2009;490:51–9.
25. Mikuli AM, Hetmanczyk J, Mikuli E, Hetmanczyk L. Thermal behaviour of polycrystalline  $[\text{Ba}(\text{H}_2\text{O})_3](\text{ClO}_4)_2$  and  $[\text{Ba}(\text{NH}_3)_4](\text{ClO}_4)_2$ . *Thermochim Acta.* 2009;487:43–8.
26. Leineweber A, Jacobs H. Preparation and crystal structure of  $\text{Ni}(\text{NH}_3)_2\text{Cl}_2$  and of two modifications of  $\text{Ni}(\text{NH}_3)_2\text{Br}_2$  and  $\text{Ni}(\text{NH}_3)_2\text{I}_2$ . *J Solid State Chem.* 2000;152:381–7.
27. Li C, Shuford KL, Chen M, Lee EJ, Cho SO. A facile polyol route to uniform gold octahedra with tailorable size and their optical properties. *ACS Nano.* 2008;9:1760–9.
28. Padhi SK. Solid state kinetics of thermal release of pyridine and morphological study of  $[\text{Ni}(\text{ampy})_2(\text{NO}_3)_2]$ ; ampy = 2-picolyamine. *Thermochim Acta.* 2006;448:1–6.
29. Green M, O'Brien P. The preparation of organically functionalized chromium and nickel nanoparticles. *Chem Commun.* 2001; 1912–3.
30. Vyazovkin S. Kinetic concepts of thermally stimulated reactions in solids: a view from a historical perspective. *Int Rev Phys Chem.* 2000;19:45–60.
31. Vyazovkin S. A unified approach to kinetic processing of non-isothermal data. *Int J Chem Kinet.* 1996;28:95–101.
32. Millan A, Clemente RR, Veintemillas S, Spinner B. Decomposition and synthesis of  $\text{NiCl}_2$  ammoniate salts: an optical microscopy study. *J Chem Soc Faraday Trans.* 1997;93(18):3363–9.
33. Vyazovkin S. Modification of the integral isoconversional method to account for variation in the activation energy. *J Comput Chem.* 2001;22:178–83.